International Journal of Modern Physics B
Vol. 33, No. 32 (2019) 1950390 (13 pages)

DOI: 10.1142/S0217979219503909

World Scientific
www.worldscientific.com

Systematic trends in $YAlO_3$, $SrTiO_3$, $BaTiO_3$, $BaZrO_3$ (001) and (111) surface *ab initio* calculations

Roberts Eglitis*, J. Purans and A. I. Popov

Institute of Solid State Physics, University of Latvia,
8 Kengaraga street, Riga LV1063, Latvia
**rieglitis@gmail.com*

Ran Jia

Laboratory of Theoretical and Computational Chemistry,
Institute of Theoretical Chemistry, Jilin University,
Changchun 130023, P. R. China
jiaran@jlu.edu.cn

Received 5 September 2019
Revised 30 October 2019
Accepted 3 November 2019
Published 31 January 2020

The paper presents and discusses the results of performed calculations for $YAlO_3$ (111) surfaces using a hybrid B3LYP description of exchange and correlation. Calculation results for $SrTiO_3$, $BaTiO_3$ and $BaZrO_3$ (111) as well as $YAlO_3$, $SrTiO_3$, $BaTiO_3$ and $BaZrO_3$ (001) surfaces are listed for comparison purposes in order to point out systematic trends common for these four ABO_3 perovskite (001) and (111) surfaces. According to performed *ab initio* calculations, the displacement of (001) and (111) surface metal atoms of $YAlO_3$, $SrTiO_3$, $BaTiO_3$ and $BaZrO_3$ perovskite, upper three surface layers for both AO and BO_2 (001) as well as AO_3 and B (111) surface terminations, in most cases, are considerably larger than that of oxygen atoms. The $YAlO_3$, $SrTiO_3$, $BaTiO_3$ and $BaZrO_3$ (001) surface energies for both calculated terminations, in most cases, are almost equal. In contrast, the (111) surface energies for both AO_3 and B-terminations are quite different. Calculated (111) surface energies always are much larger than the (001) surface energies. As follows from performed *ab initio* calculations for $YAlO_3$, $SrTiO_3$, $BaTiO_3$ and $BaZrO_3$ perovskites, the AO- and BO_2-terminated (001) as well as AO_3- and B-terminated (111) surface bandgaps are almost always reduced with respect to their bulk bandgap values.

Keywords: *Ab initio* calculation; $YAlO_3$; (111) surfaces; surface energies; B3LYP.

PACS numbers: 68.35.−p, 71.15.Mb, 71.20.−b, 73.20.At

1. Introduction

Surface and interface processes, happening in the ABO_3 perovskites and their complex nanostructures, as well as the original mechanisms of surface processes are

hot topics in modern physics nowadays.[1–18] $BaTiO_3$, $BaZrO_3$, $SrTiO_3$ and $YAlO_3$ belong to the family of ABO_3 perovskite type oxydes, and have a large number of technological applications besides being of large fundamental importance for basic research. The most important industrial applications of ABO_3 perovskites are charge storage devices, actuators, capacitors, fuel cells, water splitting applications, etc.[19–22]

Thereby, it is self-evident that their neutral and consequently rather simple (001) surfaces, during the last quarter of the century, were intensively explored worldwide, both experimentally and theoretically.[23–38] It is worth to noting that the $YAlO_3$ (001) surface is different from most ABO_3 perovskite neutral (001) surfaces, since it consists of alternating charged YO and AlO_2 (001) planes.[39]

From a theoretical point of view, it is considerably more easy to calculate the ABO_3 perovskite neutral (001) surfaces, than their complex, charged and polar (111) surfaces. This is the main reason why only a relatively small amount of theoretical and experimental papers exist dealing with ABO_3 perovskite polar, charged and thereby rather complex (111) surfaces.[40–48]

The structure of $SrTiO_3$, $BaTiO_3$, $BaZrO_3$ and $YAlO_3$ crystals in their cubic phases represent an alternating sequence of layers consisting of two kinds of atoms. Namely, the ABO_3 perovskites in the [001] direction contain alternating and neutral AO and BO_2 planes, whereas in the [111] direction, they consist of alternating charged AO_3 and B planes. For example, at high-temperatures, $BaTiO_3$ perovskite has a cubic structure with the space group Pm3m, No. 221. As temperature lowers, $BaTiO_3$ undergoes three phase transitions from cubic to tetragonal and later to orthorhombic and rhombohedral phases. From another side, the $BaZrO_3$ crystal, as temperature lowers, always stays at its high symmetry cubic phase. At room-temperature, the $SrTiO_3$ crystal has a high symmetry cubic structure.

The aim of the work reported here was to perform the first *ab initio* calculations for complex, polar and charged $YAlO_3$ (111) surfaces and compare them with earlier calculation results for related ABO_3 perovskite (001) and (111) surfaces. After performing *ab initio* calculations for $YAlO_3$ (111) surfaces, the results for $SrTiO_3$, $BaTiO_3$, $BaZrO_3$ and $YAlO_3$ (001) and (111) surfaces were analysed as well as systematic trends common for all four mentioned ABO_3 perovskites were pointed out in a form easily readable for a broad audience of researchers.

2. Technical Calculation Details

2.1. *$YAlO_3$ (111) surface atomic structure*

The main problem in modeling the $YAlO_3$ polar and charged (111) surface is that, unlike the classical ABO_3 perovskite neutral (001) surfaces, it consists from charged planes YO_3 and Al, as shown in Fig. 1, assuming standard ionic charges of Y^{3+}, Al^{3+} and O^{2-}, the $YAlO_3$ (111) surfaces have been calculated using two-dimensional slabs, containing nine planes perpendicular to the [111] $YAlO_3$ crystal direction (Fig. 1). Namely, in order to calculated the $YAlO_3$ (111) surfaces, we

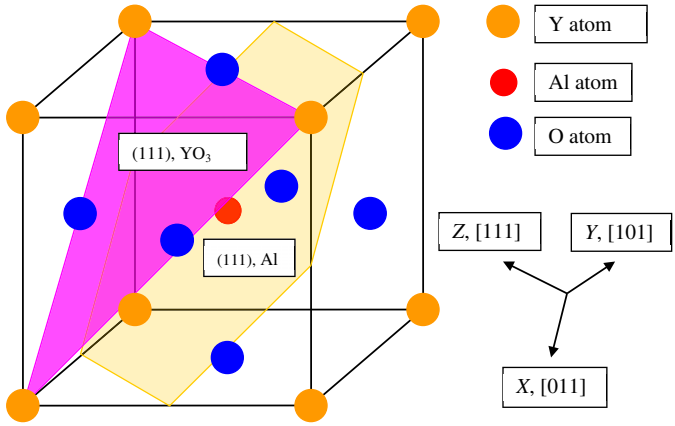

Fig. 1. (Color online) Sketch of the cubic $YAlO_3$ perovskite structure demonstrating two possible polar (111) surface terminations YO_3 and Al.

used symmetrical with respect to the mirror plane slabs consisting, in our case, from nine alternating Al and YO_3 layers. One of calculated nine layer slabs from both slab sides are terminated by Al planes and consists of a supercell containing 21 atoms (Al–YO_3–Al–YO_3–Al–YO_3–Al–YO_3–Al) [Fig. 2(a)]. The second calculated $YAlO_3$ (111) slab is terminated by YO_3 planes from both sides and consists of a supercell which contains 24 atoms (YO_3–Al–YO_3–Al–YO_3–Al–YO_3–Al–YO_3)

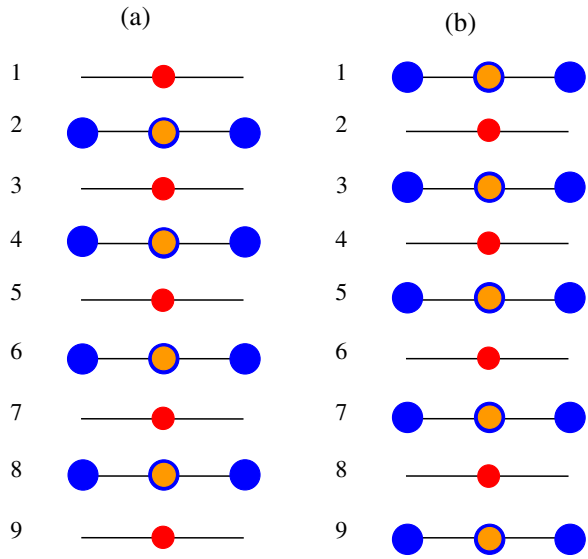

Fig. 2. (Color online) Side views of the slab geometries used by us to study the $YAlO_3$ polar (111) surfaces. (a) Nonstoichiometric Al-terminated nine layer $YAlO_3$ (111) slab and (b) nonstoichiometric YO_3-terminated nine layer $YAlO_3$ (111) slab.

[Fig. 2(b)]. Thereby, both calculated slabs are nonstoichiometric and they have unit cell formulas $Y_4Al_5O_{12}$ and $Y_5Al_4O_{15}$, respectively (Fig. 2).

As it is known from early studies dealing with $SrTiO_3$, $BaTiO_3$, $CaTiO_3$ and $BaZrO_3$ polar and charged (111) surfaces,[41,43,45,49,50] the strong electron redistribution are observed for such (111) terminations with aim to cancel the polarity, but the Al- and YO_3-terminated $YAlO_3$ (111) surface maintain its insulating character, and such calculations are possible. Of course, it is impossible to carry out calculations for asymmetric slabs with different terminations, such as, for example, Al–YO_3–Al–YO_3–Al–YO_3–Al–YO_3. Such calculations will be impossible due to a large dipole moment for an assymetric slab perpendicular to the z crystal direction.[41,43,45]

2.2. *Computational method and $YAlO_3$ (111) surface energy calculations*

Ab initio calculations for $YAlO_3$ (111) surfaces have been performed by means of the CRYSTAL computer code.[51] The most important feature of the CRYSTAL computer code for the study of the perovskite (001) and (111) surfaces is the isolated 2D slab model, which allows to perform surface calculations without artificial repetition along the z-axis. In order to perform calculations using the linear combination of atomic orbitals (LCAO) method and Gaussian-type functions (GTF) localized at atoms as the basis for an expansion of the crystalline orbitals, it is necessary to have optimized basis sets. For our $YAlO_3$ (111) surface calculations, we used exactly the same basis sets for Y, Al and O neutral atoms as in Ref. 39 for the $YAlO_3$ (001) surface atomic and electronic structure calculations. All $YAlO_3$ (111) surface calculations have been performed by means of B3LYP hybrid exchange-correlation functional including the hybrid of nonlocal Fock exact exchange, LDA exchange and Becke's gradient corrected exchange functional,[52] in combination with the nonlocal gradient corrected correlation potential by Lee *et al.*[53] The reciprocal space integration was performed by sampling the Brillouin zone of the five atom $YAlO_3$ cubic unit cell with the $8 \times 8 \times 8$ and its (111) surfaces by $8 \times 8 \times 1$ times extended Pack–Monkhorst mesh.[54] It is worth to notice that we performed calculations by means of the B3LYP functional for $YAlO_3$ (111) and (001)[39] as well as for $SrTiO_3$,[45] $BaTiO_3$[41] and $BaZrO_3$[43] (111) surfaces. For $SrTiO_3$,[29,55,56] $BaTiO_3$[5,55,56] and $BaZrO_3$[34,55,56] (001) surfaces we performed calculations using the B3PW hybrid exchange-correlation functional.

Next, we calculated the $YAlO_3$ (111) surface and cleavage energies. It is clear that Al- and YO_3-terminated $YAlO_3$ (111) surfaces are mutually complementary. Thereby, it is obvious that the cleavage energy is exactly the same for both YO_3- and Al-terminated $YAlO_3$ (111) surfaces. Therefore, the cleavage energy for the complementary surface $E_{cl}(YO_3 + Al)$ can be derived from the total energies calculated for the unrelaxed slabs from the following equation:

$$E_{cl}(YO_3 + Al) = \frac{1}{4}\left[{E_{slab}}^{unrel}(Al) + {E_{slab}}^{unrel}(YO_3) - 9E_{bulk}\right], \quad (1)$$

where ${E_{\rm slab}}^{\rm unrel}$ (Al) is our calculated total energy of unrelaxed 21-atoms containing Al-terminated $YAlO_3$ (111) slab. ${E_{\rm slab}}^{\rm unrel}$ (YO_3) is the total energy for 24-atom YO_3-terminated $YAlO_3$ (111) slab. $E_{\rm bulk}$ is the $YAlO_3$ total bulk energy per formula unit containing 5-atoms in the cubic structure. In Eq. (1) factor 9 before the $E_{\rm bulk}$ is due to the fact that 21-atom Al-terminated as well as 24-atom YO_3-terminated $YAlO_3$ (111) slabs both together contain nine 5-atom $YAlO_3$ bulk unit cells. Factor $\frac{1}{4}$ in the right side of Eq. (1) means that totally four surfaces are created due the crystal cleavage. The relevant relaxation energies for each of the surfaces can be obtained by means of the following equation:

$$E_{\rm rel}(\Psi) = \frac{1}{2}\left[{E_{\rm slab}}^{\rm rel}(\Psi) - {E_{\rm slab}}^{\rm unrel}(\Psi)\right], \tag{2}$$

where Ψ = Al or YO_3 describes the $YAlO_3$ (111) surface termination. ${E_{\rm slab}}^{\rm rel}(\Psi)$ is the Al- or YO_3-terminated $YAlO_3$ (111) slab total energy after the atomic relaxation. The ${E_{\rm slab}}^{\rm unrel}(\Psi)$ is the Al- or YO_3-terminated $YAlO_3$ (111) slab total energy before the atomic relaxation. The factor of $\frac{1}{2}$ comes from the fact that two surfaces are created due to the crystal cleavage. Finally, when we know the cleavage and relaxation energies, the surface energy is calculated as the sum of them

$$E_{\rm surf}(\Psi) = E_{\rm cl}(YO_3 + {\rm Al}) + E_{\rm rel}(\Psi). \tag{3}$$

3. *Ab Initio* Calculation Results for $YAlO_3$ (111) Surfaces. Comparison with $YAlO_3$ (001) as well as $SrTiO_3$, $BaTiO_3$ and $BaZrO_3$ (001) and (111) Surfaces

As a starting point of *ab initio* B3LYP calculations, we calculated the $YAlO_3$ bulk lattice constant (3.712 Å). We used calculated theoretical $YAlO_3$ bulk lattice constant in the following $YAlO_3$ polar (111) surface structure calculations. In order to describe the chemical bonding and covalency effects, we used the classical Mulliken bond population analysis for the atomic charges Q and bond populations P as described in Refs. 57 and 58 Calculated effective charges for the $YAlO_3$ bulk atoms are equal to (+2.523 e) for the Y atom, (+2.216 e) for the Al atom, and finally (−1.580 e) for the O atom. Calculated $YAlO_3$ bulk chemical bond population between Al and O atoms is equal to (+0.170 e), and it is considerably smaller, only (+0.010 e) between the Y and O atoms. Calculated $YAlO_3$ bulk optical band by means of the B3LYP method at Γ point is equal to 6.21 eV.

According to the results of performed calculations for Al-terminated $YAlO_3$ (111) surface (Table 1), the upper layer Al atom is strongly (by 4.85% of bulk lattice constant a_0) displaced inwards toward the bulk. The second layer metal Y atom is displaced inwards even more strongly (by 6.47% of a_0). The second layer O atom is displaced very slightly outwards (by 0.06% of a_0). The third layer Al atom, in contrast to the first layer Al atom, rather strongly (by 2.42% of a_0) is displaced outwards. As we can see from Table 1, according to performed calculations for all four materials, first and second layer metal atoms are strongly displaced inwards,

Table 1. Calculated displacement of Al-, Ti- and Zr-terminated $YAlO_3$, $SrTiO_3$, $BaTiO_3$ and $BaZrO_3$ (111) surface upper three layer atoms (as a percentage of the bulk crystal lattice constant $a_0 = 3.712$, 3.914, 4.021, 4.234 Å, respectively). Positive (negative) values describe atomic displacements in the direction outwards (inwards) of the surface.

Material		$YAlO_3$	$SrTiO_3$	$BaTiO_3$	$BaZrO_3$
Layer	Ion	Displacement (Δz)	Displacement (Δz)	Displacement (Δz)	Displacement (Δz)
1	B	−4.85	−3.58	−11.19	−8.03
2	A	−6.47	−11.24	−6.22	−9.73
	O	+0.06	+1.53	+2.74	+0.78
3	B	+2.42	+0.26	−0.25	−0.02

Table 2. Calculated displacement of YO_3-, SrO_3- and BaO_3-terminated $YAlO_3$, $SrTiO_3$, $BaTiO_3$ and $BaZrO_3$ (111) surface upper three layer atoms (as a percentage of the bulk crystal lattice constant $a_0 = 3.712$, 3.914, 4.021, 4.234 Å, respectively). Positive (negative) values describe atomic displacements in the direction outwards (inwards) of the surface.

Material		$YAlO_3$	$SrTiO_3$	$BaTiO_3$	$BaZrO_3$
Layer	Ion	Displacement (Δz)	Displacement (Δz)	Displacement (Δz)	Displacement (Δz)
1	A	−1.51	+1.33	−1.24	+1.70
	O	−0.16	−0.03	−3.98	−0.57
2	B	+0.19	+1.81	+2.49	+0.21
3	A	+0.78	−0.03	+1.49	+0.71
	O	+0.11	−0.26	−0.25	−0.01

while all second layer O atoms are displaced outwards by much smaller displacement magnitude than the metal atoms inwards.

For YO_3-terminated $YAlO_3$ (111) surface, both upper layer atoms are displaced inwards, whereas all second and third layer atoms are displaced outwards (Table 2). Namely, the upper layer metal atom Y is displaced inwards by 1.51% of a_0 and also the oxygen atom slightly, only by 0.16% of a_0, is displaced inwards. All second and third layer atoms are displaced outwards, but by rather small displacement magnitudes less than 1% of a_0 (Table 2). It is worth noting that for all four calculated perovskites (Table 2), the first layer oxygen atoms are displaced inwards, while all second layer atoms are displaced outwards.

With the aim to compare the calculated and experimental $SrTiO_3$ (001) surface structures, the surface rumpling s (the relative displacement of the metal atom with respect to oxygen in the upper surface layer) as well as the changes in the interlayer distances Δd_{ij} (where i and j are numbers of layers) are collected in Table 3. Calculated interlayer distances are based on the positions of displaced metal atoms, which as we know are much better electron scatterers than oxygen atoms.[59] As we can see from Table 3, the agreement is fairly good for all theoretical calculation methods, which give the same sign for the surface rumpling as well as the changes of the interlayer distances. For example, the surface rumpling s for the SrO-terminated surface is calculated to be much larger than for the TiO_2-terminated $SrTiO_3$ (001) surface by all theoretical methods.[60–63] As we can see from Table 3, both calculated

Table 3. Calculated and experimental surface rumpling s and relative displacements Δd_{ij} (in percent of the bulk lattice constant) for the upper three surface planes of SrO- and TiO_2-terminated $SrTiO_3$ (001) slabs.

	SrO-terminated $SrTiO_3$ (001)			TiO_2-terminated $SrTiO_3$ (001)		
$SrTiO_3$	s	Δd_{12}	Δd_{23}	s	Δd_{12}	Δd_{23}
This work	5.66	−6.58	1.75	2.12	−5.79	3.55
Shell model[60]	8.2	−8.6	3.0	1.2	−6.4	4.0
HF-LYP[61]	3.8	−4.3	1.3	1.2	−4.9	2.2
Ab initio[62]	5.8	−6.9	2.4	1.8	−5.9	3.2
Ab initio[63]	7.7	−8.6	3.3	1.5	−6.4	4.9
LEED exp[59]	4.1 ± 2	-5 ± 1	2 ± 1	2.1 ± 2	1 ± 1	-1 ± 1
RHEED exp[64]	4.1	2.6	1.3	2.6	1.8	1.3
MEIS exp[65]				1.5 ± 0.2	0.5 ± 0.2	
SXRD exp[66]	1.3 ± 12.1	-0.3 ± 3.6	-6.7 ± 2.8	12.8 ± 8.5	0.3 ± 1	

TiO_2- and SrO-terminated (001) $SrTiO_3$ surfaces exhibit a reduction of interlayer distance Δd_{12} and an expansion of Δd_{23}.

The calculated surface rumpling amplitudes s for both $SrTiO_3$ (001) surface terminations are in fair agreement with the LEED, RHEED, MEIS and SXRD experiments[59,64–66] (Table 3). Nevertheless, the calculated changes in interlayer distances are in disagreement with the LEED experiments[59] for the TiO_2-terminated $SrTiO_3$ (001) surface, which show an expansion of the Δd_{12} and a reduction of Δd_{23}. In contrast, all *ab initio* as well as classical shell model calculations show a reduction of interlayer distance Δd_{12} and an expansion of Δd_{23} (Table 3). Nevertheless, as we can see from Table 3, unfortunately, the different experiments contradict each other with respect the sign of Δd_{12} and Δd_{23} for the SrO-terminated $SrTiO_3$ (001) surface, and for sign of Δd_{23} of the TiO_2-terminated $SrTiO_3$ (001) surface.

Calculated surface relaxation energy for Al-terminated $YAlO_3$ (111) surface (−1.24 eV) is more than seventeen times larger than the surface relaxation energy for YO_3-terminated $YAlO_3$ (111) surface (−0.07 eV) (Table 4). Calculated surface energy for the YO_3-terminated $YAlO_3$ (111) surface is equal to 9.26 eV/cell and thereby it by 1.17 eV/cell exceeds the surface energy for Al-terminated $YAlO_3$ (111) surface 8.09 eV/cell (Table 4).

Calculated YO_3- and Al-terminated $YAlO_3$ (111) surface energies (9.26 and 8.09 eV/cell) (Table 4) are considerably larger than the YO- and AlO_2-terminated $YAlO_3$ (001) surface energies (2.33 and 3.31 eV/cell) (Table 5 and Fig. 3). Also for another calculated $SrTiO_3$, $BaTiO_3$ and $BaZrO_3$ perovskites, their (111) surface energies for both AO_3 and B-terminations (Table 4) are always larger than their relevant surface energies for both AO- and BO_2-terminated (001) surfaces (Table 5). From Table 4 we can see that the AO_3-terminated perovskite (111) surface energies are always larger than the B-terminated surface energies for $YAlO_3$, $SrTiO_3$, $BaTiO_3$ and $BaZrO_3$ perovskites (Table 4). It is worth noting that the ABO_3 perovskite (001) surface energies are also always smaller than the ABO_3 perovskite (011) surface energies.[16] The only exception is calculations by Zhang *et al.*,[67] where

Table 4. Calculated cleavage, relaxation, and surface energies for $YAlO_3$, $SrTiO_3$, $BaTiO_3$ as well as $BaZrO_3$ (111) surfaces (in electron volt per surface cell).

Surface (111)	E_{cl} (AO_3+B)	Termination	E_{rel}	E_{surf} (111)
$YAlO_3$	9.33	Al-terminated	−1.24	8.09
		YO_3-terminated	−0.07	9.26
$SrTiO_3$	6.65	Ti-terminated	−1.66	4.99
		SrO_3-terminated	−0.35	6.30
$BaTiO_3$	9.22	Ti-terminated	−1.94	7.28
		BaO_3-terminated	−0.82	8.40
$BaZrO_3$	9.43	Zr-terminated	−1.49	7.94
		BaO_3-terminated	−0.10	9.33

Table 5. Calculated surface energies for $YAlO_3$, $SrTiO_3$, $BaTiO_3$ as well as $BaZrO_3$ (001) surfaces (in electron volt per surface cell).

Surface (001)	Termination	E_{surf} (001)
$YAlO_3$	YO-terminated	2.33
	AlO_2-terminated	3.31
$SrTiO_3$	SrO-terminated	1.15
	TiO_2-terminated	1.23
$BaTiO_3$	BaO-terminated	1.19
	TiO_2-terminated	1.07
$BaZrO_3$	BaO-terminated	1.30
	ZrO_2-terminated	1.31

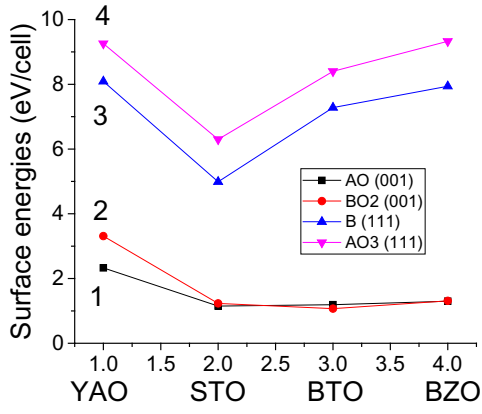

Fig. 3. (Color online) Our calculated surface energies (in eV/cell) for AO- (1) and BO_2-terminated (2) (001) as well as B- (3) and AO_3-terminated (4) (111) surfaces of $YAlO_3$, $SrTiO_3$, $BaTiO_3$ and $BaZrO_3$ perovskites by means of the hybrid B3LYP or B3PW exchange-correlation functionals.

Table 6. Calculated B–O chemical bond population of $YAlO_3$, $SrTiO_3$, $BaTiO_3$ and $BaZrO_3$ perovskite bulk, BO_2-terminated (001) as well as AO_3-terminated (111) surfaces (in e).

B–O bond population	$YAlO_3$	$SrTiO_3$	$BaTiO_3$	$BaZrO_3$
Bulk	+0.170	+0.088	+0.098	0.108
BO_2-terminated (001)	+0.232	+0.118	+0.126	0.132
AO_3-terminated (111)	+0.252	+0.098	+0.118	0.118

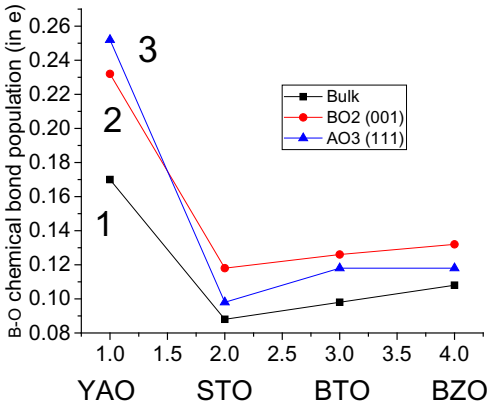

Fig. 4. (Color online) Calculated bulk (1) as well as BO_2-terminated (001) (2) and AO_3-terminated (111) surface B–O chemical bond populations (in e) for $YAlO_3$, $SrTiO_3$, $BaTiO_3$ and $BaZrO_3$ perovskites.

they found that the A-type O-terminated $CaTiO_3$ (011) surface energy is smaller than the TiO_2-terminated $CaTiO_3$ (001) surface energy.

The covalent nature of the chemical bonding between Al and O atoms in the $YAlO_3$ bulk is confirmed by the large bond population values between Al and O atoms (+0.170 e) (Table 6 and Fig. 4). This Al–O bond population valued for the $YAlO_3$ bulk is considerably larger than the relevant B–O chemical bond population for another our calculated $SrTiO_3$, $BaTiO_3$ and $BaZrO_3$ perovskites (0.088, 0.098 and 0.108 e, respectively). The Al–O chemical bond population near the AlO_2-terminated $YAlO_3$ (001) surface is 1.36 times larger than in the $YAlO_3$ bulk (Table 6). Nevertheless, the Al–O chemical bond population reach its maximal value near the YO_3-terminated $YAlO_3$ (111) surface and is equal to (0.252 e), or in another words, it is 1.48 times larger than in the $YAlO_3$ bulk. It is interesting to notice, that also for another our calculated $SrTiO_3$, $BaTiO_3$ and $BaZrO_3$ perovskites the B–O chemical bond population near the (001) and (111) surfaces is considerably larger than in the bulk. Nevertheless, for $SrTiO_3$, $BaTiO_3$ and $BaZrO_3$ perovskites, in contrast to $YAlO_3$, the B–O chemical bond population near the (001) surfaces is larger than near the (111) surfaces.

By means of the B3LYP functional calculated $SrTiO_3$ bulk bandgap (3.99 eV) is only by 0.24 eV or approximately 6.4% overestimated regarding the experimental

Table 7. Calculated optical bandgaps at the Γ-point for $YAlO_3$, $SrTiO_3$, $BaTiO_3$ and $BaZrO_3$ bulk as well as AO_3- and B-terminated (111) and BO_2- and AO-terminated (001) surfaces (in eV).

Optical bandgap	$YAlO_3$	$SrTiO_3$	$BaTiO_3$	$BaZrO_3$
Bulk	6.21	3.99	3.55	4.79
AO_3-terminated (111)	4.57	3.72	3.60	4.51
B-terminated (111)	5.95	3.98	4.14	4.47
AO-terminated (001)	6.02	3.72	3.49	4.71
BO_2-terminated (001)	6.41	3.95	2.96	4.37
Experiment	8.5[a]	3.75[b]	2.84[c]	5.3[d]

Notes: [a]Ref. 71, [b]Ref. 68, [c]Ref. 70, [d]Ref. 69.

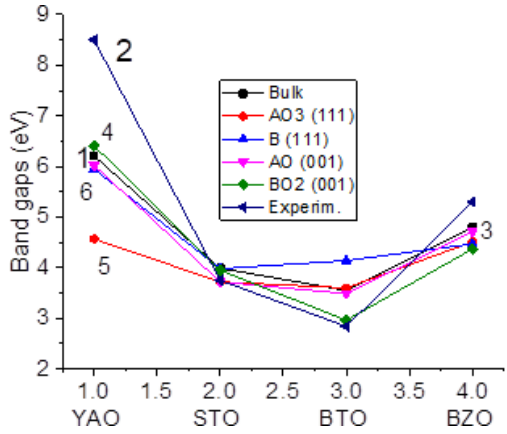

Fig. 5. (Color online) Calculated (1) and experimental (2) bulk as well as calculated AO (3) and BO_2-terminated (4) (001), AO_3 (5) and B-terminated (6) (111) surface Γ–Γ bandgaps (in eV) for $YAlO_3$, $SrTiO_3$, $BaTiO_3$ and $BaZrO_3$ perovskites.

bulk bandgap value of 3.75 eV[68] (Table 7 and Fig. 5). Also for $BaZrO_3$ bulk, by means of the B3LYP method calculated bandgap (4.79 eV) is only by 0.51 eV or 9.6% underestimated regarding the experimental bulk bandgap value of 5.3 eV[69] (Table 7). According to the recent experimental data, the $BaTiO_3$ bulk bandgap in its cubic phase is equal to approximately 2.84 eV.[70] We compared the B3LYP calculation result for $YAlO_3$ bulk bandgap in the cubic phase with the experimental result obtained for its orthorhombic phase 8.5 eV.[71]

Calculated ABO_3 optical bandgaps near the (001) surfaces as a rule are smaller than the ABO_3 perovskite bulk bandgaps. The single exception is the $YAlO_3$ perovskite AlO_2-terminated (001) surface bandgap (6.41 eV), which by 0.2 eV exceeds the $YAlO_3$ bulk bandgap value (6.21 eV). Also for $YAlO_3$, $SrTiO_3$ and $BaZrO_3$ perovskite (111) surfaces, our calculated bandgap near the (111) surfaces is reduced with respect to the bulk bandgap value. The only exception from this tendency is increase of our calculated bandgaps near the $BaTiO_3$ (111) surfaces.

4. Summary and Conclusions

We performed a large amount of B3LYP and B3PW calculations for $YAlO_3$, $SrTiO_3$, $BaTiO_3$ and $BaZrO_3$ (001) and (111) surfaces, and as a result detected following systematic trends:

(1) The relaxation of (001) and (111) surface metal atoms for $YAlO_3$, $SrTiO_3$, $BaTiO_3$ and $BaZrO_3$ perovskite, in the upper three surface layers for both AO and BO_2 (001) as well as AO_3 and B (111) surface terminations, in most cases, are considerably larger than that of oxygen atoms.
(2) For the AO- and BO_2-terminated (001) as well as AO_3- and B-terminated (111) surfaces of $YAlO_3$, $SrTiO_3$, $BaTiO_3$ and $BaZrO_3$ perovskites, the systematic trend, with a few exceptions, according to performed B3LYP and B3PW calculations, is that all atoms of the upper surface layer relax inward, whereas all atoms of the second surface layer relax outward.
(3) The $YAlO_3$, $SrTiO_3$, $BaTiO_3$ and $BaZrO_3$ (001) surface energies for both calculated AO and BO_2-terminations, in most cases, are almost equal. In contrast, the (111) surface energies for both AO_3 and B-terminations are quite different, also the AO_3-terminated (111) surface energies are always considerably larger than the B-terminated (111) surface energies. Calculated AO_3- and B-terminated (111) surface energies always are much larger than the AO- and BO_2-terminated (001) surface energies.
(4) The B–O chemical bond population in $YAlO_3$, $SrTiO_3$, $BaTiO_3$ and $BaZrO_3$ perovskite bulk are always smaller than near the (111) and especially the (001) surfaces. In most cases the B–O chemical bond population near the (001) surfaces are slightly larger than near the (111) surfaces.
(5) As follows from the performed B3LYP and B3PW calculations for $YAlO_3$, $SrTiO_3$, $BaTiO_3$ and $BaZrO_3$ perovskites, the AO- and BO_2-terminated (001) as well as AO_3- and B-terminated (111) surface bandgaps are always reduced with respect to their bulk bandgap values. The only exceptions are the $BaTiO_3$ (111) surface bandgaps as well as BO_2-terminated $YAlO_3$ (001) surface bandgaps.

Acknowledgments

We greatly acknowledge the financial support via Latvian-Ukrainian Joint Research Project No. LV-UA/2018/2, Latvian Council of Science Grant No. 2018/2-0083 "Theoretical prediction of hybrid nanostructured photocatalytic materials for efficient water splitting", Latvian Council of Science Grant No. 2018/1-0214 as well as ERAF Project No. 1.1.1.1/18/A/073.

References

1. M. Dawber, K. M. Rabe and J. F. Scott, *Rev. Mod. Phys.* **77**, 1083 (2005).
2. S. E. Reyes-Lillo, K. M. Rabe and J. B. Neaton, *Phys. Rev. Mater.* **3**, 030601 (2019).

3. Y. A. Mastrikov *et al.*, *J. Mater. Chem. A* **6**, 11929 (2018).
4. C. G. Ma, V. Krasnenko and M. G. Brik, *J. Phys. Chem. Solids* **115**, 289 (2018).
5. R. I. Eglitis and D. Vanderbilt, *Phys. Rev. B* **76**, 155439 (2007).
6. W. Jia *et al.*, *J. Lumin.* **83–84**, 109 (1999).
7. J. Meng *et al.*, *J. Mater. Sci.* **54**, 1967 (2019).
8. R. I. Eglitis, *Int. J. Mod. Phys. B* **28**, 1430009 (2014).
9. R. A. P. Ribeiro *et al.*, *Appl. Surf. Sci.* **452**, 463 (2018).
10. B. C. Luo *et al.*, *Appl. Surf. Sci.* **351**, 558 (2015).
11. R. Eglitis, *Int. J. Mod. Phys. B* **33**, 1950151 (2019).
12. Z. Zhao *et al.*, *Phys. Rev. Mater.* **3**, 043601 (2019).
13. M. Sokolov *et al.*, *Int. J. Mod. Phys. B* **31**, 1750251 (2017).
14. E. A. Kotomin *et al.*, *Phys. Chem. Chem. Phys.* **10**, 4258 (2008).
15. M. V. Ananev *et al.*, *Russ. J. Electrochem.* **48**, 879 (2012).
16. R. I. Eglitis *et al.*, *J. Mater. Sci.* **55**, 203 (2020).
17. N. M. Porotnikova, M. V. Ananev and E. Kh. Kurumchin, *Russ. J. Electrochem.* **47**, 1250 (2011).
18. R. I. Eglitis and A. I. Popov, *J. Nano-Electron. Phys.* **11**, 01001 (2019).
19. H. Y. Hwang *et al.*, *Nat. Mater.* **11**, 103 (2012).
20. T. Matsuda *et al.*, *J. Alloys Compd.* **351**, 43 (2003).
21. Z. Zhang *et al.*, *Adv. Energy Mater.* **7**, 1700242 (2017).
22. A. A. Emery and C. Wolverton, *Sci. Data* **4**, 170153 (2017).
23. K. Szot *et al.*, *Appl. Phys. A* **62**, 335 (1996).
24. J. Druce *et al.*, *Energy Environ. Sci.* **7**, 3593 (2014).
25. G. Z. Zhu, G. Radtke and G. A. Botton, *Nature* **490**, 384 (2012).
26. M. S. J. Marshall *et al.*, *Phys. Rev. B* **83**, 035410 (2011).
27. Y. Y. Lin *et al.*, *Surf. Sci.* **605**, L51 (2011).
28. R. Shimizu *et al.*, *Appl. Phys. Lett.* **100**, 263106 (2012).
29. R. I. Eglitis and D. Vanderbilt, *Phys. Rev. B* **77**, 195408 (2008).
30. R. I. Eglitis and D. Vanderbilt, *Phys. Rev. B* **78**, 155420 (2008).
31. M. G. Brik, C. G. Ma and V. Krasnenko, *Surf. Sci.* **608**, 146 (2013).
32. E. A. Kotomin *et al.*, *Thin Solid Films* **400**, 76 (2001).
33. K. Yang *et al.*, *Int. J. Mod. Phys. B* **30**, 1650168 (2016).
34. R. I. Eglitis, *J. Phys.: Condens. Matter* **19**, 356004 (2007).
35. M. Saghayezhian *et al.*, *J. Phys. Chem. C* **123**, 8086 (2019).
36. R. I. Eglitis and A. I. Popov, *J. Saudi Chem. Soc.* **22**, 459 (2018).
37. J. R. Sambrano *et al.*, *J. Mol. Struct.* **813**, 49 (2007).
38. G. Borstel *et al.*, *Phys. Stat. Sol. B* **236**, 253 (2003).
39. R. I. Eglitis and A. I. Popov, *Nucl. Instr. Meth. B* **434**, 1 (2018).
40. N. Sivadas *et al.*, *Phys. Rev. B* **89**, 075303 (2014).
41. R. I. Eglitis, *Appl. Surf. Sci.* **358**, 556 (2015).
42. W. Liu *et al.*, *Solid State Commun.* **149**, 1871 (2009).
43. R. I. Eglitis, *Solid State Ion.* **230**, 43 (2013).
44. J. Feng, X. Zhu and J. Guo, *Surf. Sci.* **614**, 38 (2013).
45. R. I. Eglitis, *Phys. Stat. Sol. B* **252**, 635 (2015).
46. Y. Liang *et al.*, *Sci. Rep.* **5**, 10634 (2015).
47. R. I. Eglitis, *Ferroelectrics* **483**, 53 (2015).
48. G. M. Vanacore, L. F. Zagonel and N. Barrett, *Surf. Sci.* **604**, 1674 (2010).
49. A. Pojani, F. Finocchi and C. Noguera, *Surf. Sci.* **442**, 179 (1999).
50. A. Pojani, F. Finocchi and C. Noguera, *Appl. Surf. Sci.* **142**, 177 (1999).
51. V. R. Saunders *et al.*, *CRYSTAL User Manual* (University of Torino, Italy, 2009).

52. A. D. Becke, *J. Chem. Phys.* **98**, 5648 (1993).
53. C. Lee, W. Yang and R. G. Parr, *Phys. Rev. B* **37**, 785 (1988).
54. H. J. Monkhorst and J. D. Pack, *Phys. Rev. B* **13**, 5188 (1976).
55. R. I. Eglitis *et al.*, *Ceram. Int.* **30**, 1989 (2004).
56. S. Piskunov *et al.*, *Surf. Sci.* **575**, 75 (2005).
57. C. R. A. Catlow and A. M. Stoneham, *J. Phys. C: Solid State Phys.* **16**, 4321 (1983).
58. R. C. Bochiccio and H. F. Reale, *J. Phys. B: At. Mol. Opt. Phys.* **26**, 4871 (1993).
59. N. Bickel *et al.*, *Phys. Rev. Lett.* **62**, 2009 (1989).
60. E. Heifets, E. A. Kotomin and J. Maier, *Surf. Sci.* **462**, 19 (2000).
61. E. Heifets *et al.*, *Phys. Rev. B* **64**, 235417 (2001).
62. J. Padilla and D. Vanderbilt, *Surf. Sci.* **418**, 64 (1998).
63. C. Cheng, K. Kunc and M. H. Lee, *Phys. Rev. B* **62**, 10409 (2000).
64. T. Hikita *et al.*, *Surf. Sci.* **287–288**, 377 (1993).
65. A. Ikeda *et al.*, *Surf. Sci.* **433**, 520 (1999).
66. G. Charlton *et al.*, *Surf. Sci.* **457**, L376 (2000).
67. M. Zhang *et al.*, *Phys. Rev. B* **76**, 115426 (2007).
68. K. van Benthem, C. Elsässer and R. H. French, *J. Appl. Phys.* **90**, 6156 (2001).
69. J. Robertson, *J. Vacuum Sci. Technol. B* **18**, 1785 (2000).
70. V. Mishra *et al.*, *J. Appl. Phys.* **122**, 065105 (2017).
71. C. Lushchik *et al.*, *J. Phys.: Condens. Matter* **6**, 11187 (1994).

Institute of Solid State Physics, University of Latvia as the Center of Excellence has received funding from the European Union's Horizon 2020 Framework Programme H2020-WIDESPREAD-01-2016-2017-TeamingPhase2 under grant agreement No. 739508, project CAMART²